B. Franzelli, L. Tardelli, M. Stöhr, K.P. Geigle, P. Domingo, Assessment of LES of intermittent soot production in an aero-engine model combustor using high-speed measurements, Proc. Combust. Inst. 39 (2023) 4821-4829.

The original publication is available at www.elsevier.com

http://dx.doi.org/10.1016/j.proci.2022.09.060/

Assessment of LES of intermittent soot production in an aero-engine model combustor using high-speed measurements

B. Franzelli[a], L. Tardelli[a], M. Stöhr[b], K.P. Geigle[b], P. Domingo[c]

[a] *Laboratoire EM2C, Université Paris-Saclay, CNRS, CentraleSupélec, 8-10 rue du Joliot Curie, 91190 Gif-sur-Yvette, France*
[b] *German Aerospace Center (DLR), Institute of Combustion Technology, Pfaffenwaldring 38–40, 70569 Stuttgart, Germany*
[b] *CORIA – CNRS, Normandie Université, INSA Rouen Normandie, Saint-Etienne-du-Rouvray 76801, France*

Abstract

Soot production in turbulent flames is an extremely intermittent phenomenon since it is the result of specific thermochemical conditions occasionally occurring in space and time. In realistic configurations such as the swirling flames used in gas-turbines, the presence of large-scale flow motions can additionally affect soot formation processes, leading to even more pronounced intermittency. Classically, the validation of numerical simulations is performed by comparing time-averaged results with experimental data of the phenomenon under investigation. This comparison can be considered as rigorous only if a statistically converged numerical representation is obtained. In case of sporadic events such as intermittent soot formation in turbulent flames, this means to perform the simulation over thousands of milliseconds of physical time, which can have extremely high CPU demands when performing Large Eddy Simulation (LES). In this work, a possible strategy to overcome this issue is proposed based on the use of high-speed measurements and numerically synthesized signals from LES. To illustrate the approach, numerical and experimental soot light scattering signals are considered here by looking at the model aero-engine combustor developed at DLR for the study of pressurized swirled sooting flames. The light scattering signal is numerically synthesized from an LES. Experimental high-speed measurements are used to statistically account for the high temporal and spatial variability of soot when considering time intervals similar to what is today achievable with LES. The feasibility of this approach is finally demonstrated by comparing numerical results to the ensemble of possible soot production states observed experimentally in the DLR burner allowing to eventually validate the present LES results.

Keywords: High-speed measurements; sooting flames; LES; light scattering; intermittency

1. Introduction

Soot production modeling represents a difficult challenge for turbulent combustion research. The intricate multi-scale coupling between the classical scales range of turbulent gaseous combustion and much longer soot production processes introduces time-history and large-scale effects into the problem leading to an intermittent soot presence [1–8]. When considering realistic configurations, such as swirled flames in gas turbines, soot formation is usually affected also by the presence of long time-scale flow motions. As an example, in the DLR model combustor [9], the presence of a precessing vortex core (PVC) affects the mixture in the primary combustion zone by interacting with the fuel injection. As a consequence, soot production, which strongly depends on the local conditions of the gas mixture, evolves intermittently in space and time [10–12]. In addition, the dynamics of secondary air jets, characterized by much longer times compared to the PVC, have an impact on the flow structure and, consequently, on soot production [11, 12]. The interaction between unsteady flow phenomena and long time scales for soot production leads to an even more pronounced intermittent soot presence. It is well known that the intermittent nature of soot production in turbulent flames poses a challenge for achieving statistically converged fields with Large Eddy Simulation (LES) [12]. However, a common practice to validate the simulation consists in verifying a satisfactory agreement between time-averaged experimental and numerical soot volume fraction (SVF) fields [13–18]. In reality, simulations and low-speed measurements classically represent very different physical time intervals. Therefore, their comparison may be not adequate if the characteristic time scales of the process under investigation are long and if the studied events are sporadic, such as soot production in realistic configurations. On the one side, low-speed measurements are usually performed over hundreds of seconds, so that they are capable to provide a statistical representation of soot formation processes. On the other side, LES is usually performed over tens or hundreds of milliseconds, corresponding to some flow times. This may be insufficient to statistically characterize soot events. Unfortunately, attaining the statistical temporal convergence of the numerical fields may be unaffordable in the case of LES due to CPU costs [12, 16].

In this framework, the objectives of this work are twofold. First, we consider high-speed light scattering (LS) measurements to experimentally prove that this issue is not a numerical artefact, but that it is intrinsically linked to the soot intermittent nature. High-speed LS measurements will also allow to quantify the variability of time-averaged experimental fields when considering small time intervals similar to what can be investigated today with LES. Second, we propose to change the validation paradigm by considering the results of an LES as one realization of a statistical ensemble of possible time-averaged experimental states.

After presenting the experimental setup in Sec. 2, the variability of time-averaged soot fields is discussed in Sec. 3 by considering low-speed and high-speed measurements together with LES results. Subsequently, a new post-processing strategy is proposed in Sec. 4 to provide a consistent comparison of experimental and numerical data based on high-speed measurements and on numerically synthesized LS signals from LES results. Finally, results are presented in Sec. 5 by discussing the variability of time-averaged experimental signals when considering small time intervals, by creating confidence charts from high-speed measurements and by using them to assess the LES results.

2. Experimental and numerical setups

In this work, the DLR chamber, described in detail in [19], is considered as a model combustor for the investigation of soot production in swirling pressurized flames. The primary combustion zone is fed by three concentric nozzles. Room-temperature air is introduced through a central and an annular nozzle. Ethylene is injected in between both air flows. The combustion chamber is 120 mm high and it has a square cross section of 68×68 mm^2. The injector features a primary combustion zone enveloping the injected fresh gases where these interact with the recirculated hot exhaust gases of the inner recirculation zone [19]. Each of the corner posts has an additional air duct for the injection of secondary air into the combustor at a height of 80 mm. The operation point considered for the current study is the so-called reference case, operated at 3 bar, with an equivalence ratio of 1.2 (32.2 kW) in the primary zone. A 40% air addition through the secondary air inlets is considered resulting in a global value of 0.86 at 39.3 kW.

When generating an experimental database on sooting turbulent flames, laser-induced incandescence (LII) measurements are classically employed to obtain time-averaged SVF fields [20]. Even if feasibility of application at high-speed has been proven [21, 22], this technique is classically performed at low-frame rate to avoid non-linear effects caused by multiple exposure of soot to high power laser pulses. In the following, LII measurements published in [23] are considered, which were acquired at a rate of 3 Hz. Approximately 400 images, i.e. roughly 2 minutes of acquisition, were recorded. Soot LS measurements obtained from a high-speed PIV image sequence recorded within a previous study [10] are also considered. The sequence was recorded at a rate of 9.3 kHz over a duration of approximately 2 s corresponding to 20000 images. The field of view covers an area of 44×36 mm^2 in the primary reaction zone of the burner and the pixel resolution is Δx=85 μm. The raw PIV images contain both dotted patterns of Mie scattering from PIV particles as well as the Rayleigh scattering signals from clouds of soot particles, which appear rather smooth. A specific image processing routine was developed and applied to

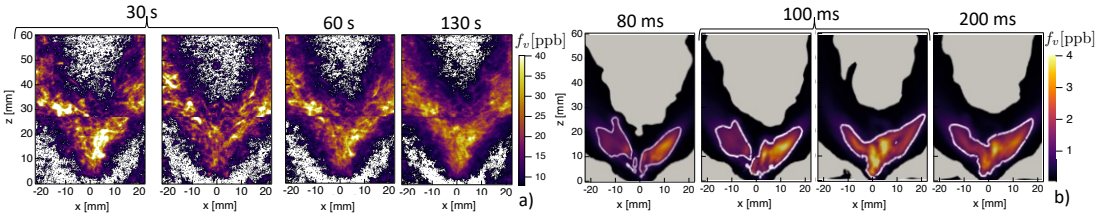

Fig. 1: Time-averaged soot volume fraction fields. a) Experimental LII data and b) LES results are time-averaged over different time-averaging interval t_{av}. White isolines of soot volume fraction (f_v=1 ppb) have been added to LES results. Note that the physical time scales covered have to be different due to nature of low-speed measurements and LES.

discriminate the dotted regions representing PIV particles and smooth soot structures [10]. The primary focus of the original work was application of stereo PIV, and information on soot scattering was derived as unexpected side-product. Thus, the laser sheet profile was not recorded and, consequently, image correction for the sheet profile of the kHz data to obtain quantitative interpretation of the LS signal is not possible.

The LES results considered in this work correspond to the simulation already presented in [12], that have been additionally performed over 300 ms using the AVBP solver [24]. Statistics were collected over the last 200 ms. The considered temporal interval is longer than the time interval considered in most LES of the DLR burner found in literature [13–15, 17, 18], which report less than 60 ms, except for 200 ms considered in [16]. The retained numerical setup has already been evaluated in [12] and is briefly summarized in supplementary materials for completeness. It accounts for low CPU-cost, yet quite accurate models: the RFPV tabulation model for the gas phase [25], a three-equation model for soot [17], an optically thin model for radiation and wall temperature from experiments imposed as boundary conditions [26]. Still, 45000 CPU hours (run on Intel E5-1920 processors) are required to obtain 10 ms of physical time. It should be noted that the target of the presented work is not the validation of the individual experimental or numerical approaches as those have already been published recently, but rather employ those existing data for an innovative approach of comparison.

3. Variability of time-averaged soot fields

Time-averaged soot volume fraction f_v fields in the DLR burner obtained from low repetition rate measurements [11] and LES are presented in Fig. 1. Different time-averaging intervals t_{av} were considered (30 s, 60 s and 130 s) by averaging 100, 200 or 400 statistically independent instantaneous LII images. The 30-seconds plot is showing distributions for two different averaging windows within the sequence. It can be observed that increasing the number of images from 100 to 400 does not change the shape of the soot distribution but rather increases the smoothness of the averaged information due to a lower weight of individual soot events. The time-averaged SVF field obtained with low-speed LII measurements can be considered as statistically converged using 400 uncorrelated images.

To quantify the effect of soot intermittency on soot statistics in the simulations, different values of time averaging t_{av} have been considered (80, 100 and 200 ms) to create time-averaged SVF fields in Fig. 1b, together with an isoline of f_v=1 ppb. A correct localization of soot production is obtained but soot load and spatial distribution evolve with time averaging. The convergence of SVF field thus has not been reached after t_{av}=100 ms. By comparing the SVF between experiments and simulations, a factor of approximately eight is observed. However, such discrepancy does not lead to any rigorous conclusion on LES quality since the presented time-averaged numerical fields are not statistically converged.

To verify that the trends observed in the simulations correspond to a real physical feature of soot production in the DLR burner, high-speed LS measurements are presented next. Results for two different time-averaging periods each at t_{av}=100 ms and 1 s are plotted in Fig. 2. Time-averaged fields strongly differ when considering two different intervals of 100 ms (Fig. 2a). Even worse, experimental results are not converged even for t_{av}=1 s (Fig. 2b). The physical processes underlying soot production thus have to be considered over longer times to obtain a statistical representation. This is because the selected configuration presents low frequency flow features and soot events are observed only for very specific thermochemical conditions of the gaseous phase, whose statistical representation requires a long time-averaging period [12]. To obtain a rigorous validation of simulations, the LES would have to be performed over thousands of milliseconds. This, however, is currently out of scope for such a complex, yet technically relevant case due to unaffordable high CPU cost.

4. Assessment of numerical results for small time-averaging intervals

The classical procedure for the validation of LES results consists in comparing time-averaged fields obtained with the numerical simulation to time-averaged experimental data. Based on the plots discussed in

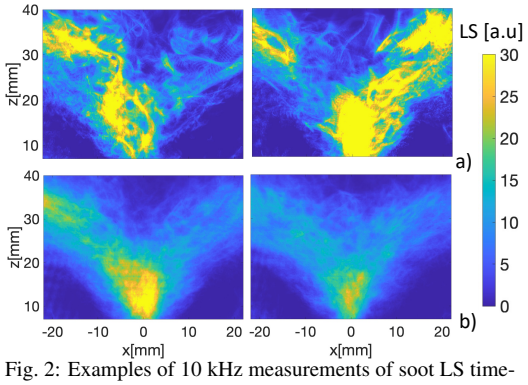

Fig. 2: Examples of 10 kHz measurements of soot LS time-averaged over a) t_{av}=100 ms and b) 1 s.

the previous section, it is evident that such comparison is not meaningful for small time-averaging intervals usually considered in LES due to the lack of temporal convergence for the SVF field in the DLR burner. Therefore, to allow the validation of LES for intermittent soot production in realistic configurations for an affordable CPU cost, we propose to change the validation paradigm by accounting for the variability of time-averaged soot quantities when small time-averaging intervals t_{av} are considered due to computational constraints.

For this purpose, high-speed LS measurements are used to create a statistical representation of the possible time-averaged states that can be experimentally observed. Then, an LES result can be considered as valid if it is one realisation of this statistical ensemble, i.e. it belongs to the confidence chart created from experiments. For this, two elements are developed in this section. First, since the available LS signals do not provide access to a physical quantity in a straightforward manner, a procedure is proposed to numerically synthesize an LS signal from LES results while adopting common temporal and spatial resolutions between the experiments and the simulation. Second, a statistical treatment of the experimental data is described to account for the variability of time-averaged LS signals when considering small t_{av} intervals.

4.1. Numerically synthesized LS signal

Comparing an experimental to a numerically synthesized signal can be a challenging task [27, 28]. Results may depend on experimental uncertainties and limits of the optical setup that have to be correctly accounted for by the numerical synthesis of the signal. In addition, differences for temporal and spatial resolutions between the experiments and the simulation have to be minimized. From the present LES, 1000 instantaneous fields have been collected over the last t_{av} =100 ms with a frequency of 10 kHz in analogy with the experimental procedure. In case of spherical particles, the LS signal can be considered as proportional to $N_p d_p^6$, with number density of particles N_p and particle diameter d_p. When considering aggregates, the LS signal depends on the morphology of the particles. Since at this stage we are only interested in quantifying the physical time needed to obtain a statistically converged LS signal, a sphericity assumption is retained when synthesizing the LS signal: $S \propto N_p v_p^2$, where $v_p = f_v/N_p$ is the particle volume. This assumption can be considered as acceptable due to the expected small size of the particles in this configuration [17, 18]. To obtain a consistent treatment of experimental and numerically synthesized signals, four post-processing steps are proposed and will also be applied identically to the experimental signals (except step 1):

1. The numerically synthesized LS signal is interpolated over the experimental grid corresponding to the camera resolution Δx.
2. The obtained interpolated signals are then filtered with a Gaussian filter of size Δ to obtain a spatial resolution larger than LES and experimental grids.
3. The 2-D data are then normalized by the instantaneous maximum value. This is done to mitigate the effect of assuming spherical particles, that can strongly impact the signal reconstruction since its intensity can be high for big particle diameters.
4. Normalized signals smaller than an arbitrary cut-off ϵ are imposed to zero, in order to artificially impose a similar 'noise' thresholding level for experimental and numerical data. The instantaneous intermittency index $\mathcal{I}$ is defined as $\mathcal{I}$=1 if $S > 0$ and $\mathcal{I}$=0 otherwise.

By doing so, it is accepted that the minimum and maximum considered values for the LS intensity, i.e. the minimum and maximum values of the particle size, may change between images. In this sense, it is only possible to identify regions where the LS signal, meaning particle size, is generally higher compared to other zones. In this case, a value of ϵ=0.005 has been chosen. A filter size of Δ=16 Δx is retained, knowing that the spatial resolution of the numerical grid in the primary zone varies between Δx and $10\Delta x$. The effect of the choice of these parameters on the time-averaged fields is discussed in the supplementary material; it has been verified that this choice does not qualitatively modify the results.

The time-averaged synthesized LS signal, illustrated in Fig. 3, is obtained by considering the 1000 instantaneous fields. It is neither symmetric nor smooth, similarly to the experimental data averaged over a short t_{av}=100 ms in Fig. 2. When looking at instantaneous synthesized LS signal and particle volume fields (an example is provided in the supplementary material), it can be observed that the LS signal has a similar distribution as the particle volume. This is expected since the LS signal is proportional to d_p^6. Therefore, the normalized LS can be reasonably used as a tracer of zones of small or big particles.

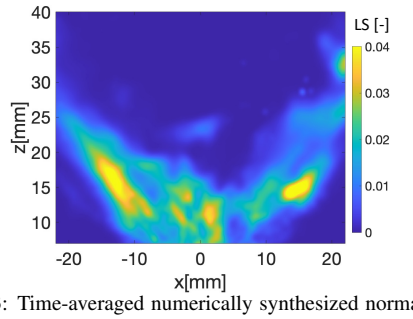

Fig. 3: Time-averaged numerically synthesized normalized LS signal for t_{av}=100 ms.

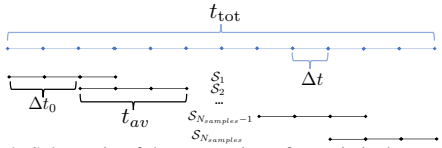

Fig. 4: Schematic of the generation of a statistical ensemble $\boldsymbol{\mathcal{S}}(t_{\text{av}}, \Delta t_0)$ of N_{samples} subsets of possible time-averaged signals $\mathcal{S}_l$.

4.2. Sampling of time-averaged experimental signal

In [10], experimental LS signals were acquired over t_{tot}=2 s with a temporal resolution of $\Delta t \approx$0.1 ms. First, the post-processing steps (2-4) used for the numerical data are applied to the experimental database to obtain normalized filtered LS and intermittency signals. Then, a statistical ensemble composed of N_{samples} subsets of time-averaged signals collected over a period t_{av} is generated. A schematic representation of the procedure is illustrated in Fig. 4. Each sample is composed of $N_{\text{im/sample}} = t_{\text{av}}/\Delta t$ images. To obtain N_{samples} subsets, the starting time of each sample is delayed by $\Delta t_0 = (t_{\text{tot}} - t_{\text{av}})/N_{\text{samples}}$, so that two consecutive subsets overlap over $t_{\text{av}} - \Delta t_0$. The final statistical ensemble of LS signals $\boldsymbol{\mathcal{S}}(t_{\text{av}}, \Delta t_0)$ accounts for N_{samples} subsets that are stored into 3-D matrices $\mathcal{S}^l_{ijk} \in \mathbb{R}_+^{N_x \times N_y \times N_{\text{im/sample}}}$ for $l = 1..N_{\text{samples}}$ and $N_x = N_y$=1024. The time-averaged ensemble of LS signal S is then obtained as:

$$\bar{S}^l_{ij} = \frac{1}{N_{\text{im/samples}}} \sum_{k=1}^{N_{\text{im/samples}}} S^l_{ijk} \quad \text{for} \quad l = 1...N_{\text{samples}}. \tag{1}$$

The time-averaged ensemble of LS signal weighted by soot presence will read as $\bar{S}^l_w = \bar{S}^l/\bar{\mathcal{I}}^l$ for $l = 1..N_{\text{samples}}$. The standard deviation ensemble of LS signal is given by: $\bar{\Sigma}^l = \sqrt{\overline{(S^l)^2} - (\bar{S}^l)^2}$ for $l = 1..N_{\text{samples}}$. Due to the normalization step in post-processing, time-averaged intermittency can be interpreted as the probability of observing soot particles. The weighted LS signal provides an indication of the spatial zones where a higher LS signal is most probably observed, possibly relating to the presence of zones of big particles.

5. Results

To quantify the fluctuations of the experimental LS signal, four different time-averaged $\bar{S}^l(t_{\text{av}}, \Delta t_0)$ ensembles with increasing time-averaging period t_{av}=50, 100, 200 and 500 ms are considered by choosing the delay between starting instants equal to Δt_0=10 ms. The observed profiles of $\bar{S}^l$ along the burner centerline (x=0 mm) are plotted in Fig. 5 coloured by their probability density. The time-averaged LS field obtained by using the entity of available images, i.e. t_{av}=2 s, is considered as the reference field that is statistically converged in time. Its profile along the burner centerline is included as a green line. First, a large scatter around the reference solution is observed for the smallest t_{av} values, proving that a high fluctuation up to a factor of six characterizes time-averaged experimental LS signals compared to the converged profile. The reference solution is located in the most probable region. For large heights above the burner z the time-averaged reference solution seems to be dominated by individual outliers, i.e. the PDF appears to peak at lower intensities. As expected, the region of possible time-averaged states becomes thinner and thinner while increasing the considered time-averaging period, demonstrating that experimental time-averaged results are slowly converging in time. The obtained ranges can be considered as confidence regions where LES results are acceptable since they reproduce a possible state of soot distribution experienced by the burner. Since the confidence area reduces when increasing the time-averaged period t_{av}, it becomes possible to validate the LES prediction with more and more accuracy by increasing the computed physical time.

The same analysis has been performed for time-averaged ensembles of LS intermittency $\bar{\mathcal{I}}^l$ and weighted LS signal $\bar{\mathcal{S}}^l_w$. Results are presented in Fig. 6 for two time-averaging intervals. A similar behaviour as for the LS signal can be observed for the intermittency (Fig. 6a), possibly indicating that the spatial distribution and the fluctuations of time-averaged LS signal are strongly correlated with time-averaged soot intermittency. The weighted LS signal in Fig. 6b presents a quite different profile. First, a spatially constant value is observed along the combustor axis, indicating that there is no privileged region for observing high LS intensity. This means that no correlation between particle size and spatial position is observed in the primary reaction zone of the burner. Second, it can be observed that the dispersion of the $\bar{\mathcal{S}}^l_w$ ensemble increases with z, especially at small t_{av}. This is due to the fact that soot presence is rare at high z, so that temporal statistics are performed over an extremely small number of samples, which leads to a strong dispersion of time-averaged profile for $\bar{\mathcal{S}}^l_w$ since it is weighted by soot presence. Overall, the proposed statistical representation allows

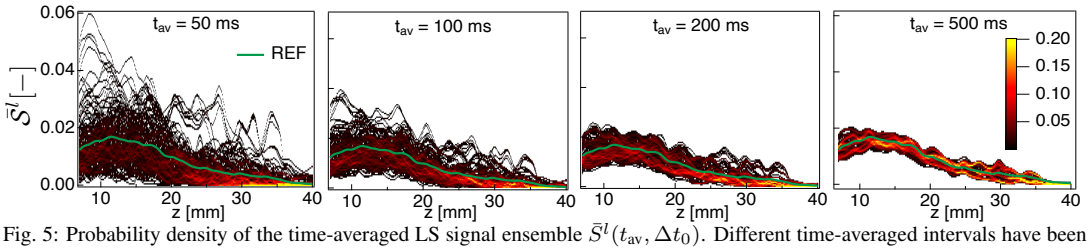

Fig. 5: Probability density of the time-averaged LS signal ensemble $\bar{S}^l(t_{\mathrm{av}}, \Delta t_0)$. Different time-averaged intervals have been considered: t_{av}=50, 100, 200, 500 ms for Δt_0=10 ms. The profiles at the centerline are illustrated together with the green line corresponding to the statistically converged reference data (t_{av}=2 s).

to quantify the high variability of soot quantities when they are time-averaged over small time intervals. This is due to the intermittent nature of soot production in realistic configurations. It also demonstrates that temporal convergence can be reached when observing soot production over a sufficiently long time, providing an indication of the time scales of soot production processes in the considered configuration. This information is not available from low-repetition rate measurements. Finally, the statistical representation of the possible time-averaged states can be used to validate LES of soot production, as done in the following.

5.1. Comparison with LES results

In Fig. 7a, the profile of the time-averaged simulated LS signal along the burner centerline from LES shown in Fig. 3 is plotted in blue symbols and line. The experimental probability density for $\bar{S}^l$ for t_{av}=100 ms and the statistically converged experimental reference solution (green line) are also represented. The approach classically considered for numerical validation would compare the two lines, corresponding to the time-averaged solution from LES and the statistically converged experimental profile.

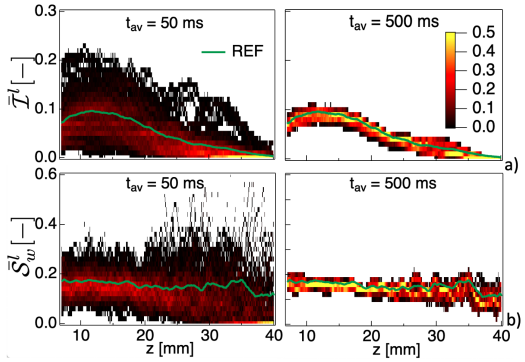

Fig. 6: Probability density of time-averaged a) intermittency $\bar{\mathcal{I}}^l$ and b) weighted LS signal $\bar{\mathcal{S}}^l_w$ ensembles for time-averaged intervals t_{av}=50 and 500 ms. Profiles along the burner centerline are represented together with the statistically converged reference profile (t_{av}=2 s, green line).

Significant discrepancies are observed, so that the LES would be assessed as insufficiently accurate. When comparing LES results to the experimental PDF of $\bar{S}^l$ ensembles generated over the same averaging period (t_{av}=100 ms) in Fig 7a, the conclusion is different. The numerical result is now enclosed in the envelope of the possible experimental states, i.e. in the experimental confidence interval. Therefore, the LES result should in principle be considered as valid. However, since the LES profile does not belong to the most probable region, the accuracy of the LES should be evaluated with caution.

The LES profile along the burner centerline for the standard deviation of the numerically synthesized LS signal is plotted in Fig. 7b, together with the standard deviations for the temporally converged experimental state and the PDF for the $\bar{\Sigma}^l$ ensemble. Conventionally, the conclusion would be that the LES result is not in agreement with experiment. However, when the variability of the standard deviation profile $\bar{\Sigma}^l$ for small averaging intervals is accounted for, the numerical simulation is valid since it represents a possible state for soot distribution in the burner. Again, the reproduced state is quite unlikely to be observed in the experiments, possibly questioning the representativeness of the LES result.

The radial profiles of $\bar{\mathcal{S}}^l$, $\bar{\mathcal{I}}^l$ and $\bar{\mathcal{S}}^l_w$ for t_{av}=100 ms at three heights above the burner (z=10, 20 and 30 mm) are finally considered in Fig. 8. Profiles of time-averaged LES and statistically converged refer-

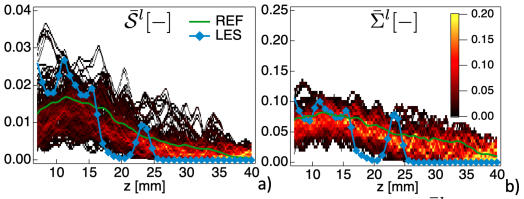

Fig. 7: Probability density of a) time-averaged $\bar{\mathcal{S}}^l$ and b) standard deviation $\bar{\Sigma}^l$ ensembles for t_{av}=100 ms. Profiles along the burner centerline are represented together with the experimental statistically converged reference data (t_{av}=2 s, green line) and the LES solution for t_{av}=100 ms (blue line and symbols).

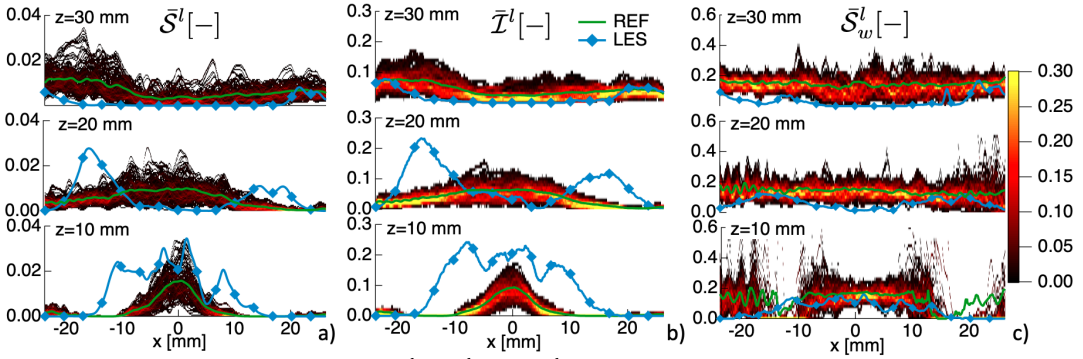

Fig. 8: Experimental probability density of a) $\bar{\mathcal{S}}^l$, b) $\bar{\mathcal{I}}^l$ and c) $\bar{\mathcal{S}}^l_w$ ensembles along the radial position for t_{av}=100 ms at three heights above the burner z=10, 20 and 30 mm. The statistically converged experimental profiles and time-averaged numerical results are also plotted as green line and blue line and symbols, respectively.

ence experimental results are also shown. First, a significant dispersion is observed experimentally, indicating a strong fluctuation in time for time-averaged quantities when considering time intervals of 100 ms. This demonstrates once again that soot-related processes in realistic configurations are an extremely intermittent phenomenon, characterized by long time scales. Therefore, a straightforward comparison between LES and experimental profiles time-averaged over different temporal periods is not rigorously meaningful. Second, a strong correlation is once again identified between the $\bar{\mathcal{S}}^l$ and $\bar{\mathcal{I}}^l$ ensembles. This indicates that the spatial distribution and temporal fluctuations of the time-averaged LS field are strongly governed by intermittency. On the contrary, the weighted LS signal $\bar{\mathcal{S}}^l_w$ presents an almost flat profile, with a similar high dispersion for each z-position. Therefore, the variability of time-averaged representations does not seem to depend on the axial position. This means that in this burner the characteristic time scale of soot-related process does not depend on the axial and radial position at least when looking at the primary combustion zone. Third, concerning the comparison with LES, an acceptable agreement is obtained close to the burner centerline for $z \leq 20$ mm when considering $\bar{\mathcal{S}}^l$ as criterion in Fig. 8a. On the contrary, a too high synthetic LS intensity is observed for $|x| > 10$ mm. This is confirmed by regarding $\bar{\mathcal{I}}^l$ in Fig. 8b, which clearly illustrates that the LES predicts a more frequent presence of soot particles in a region where almost no sooting events are experimentally observed ($|x| > 10$ mm for z =10 mm). Finally, the weighted LS signal from LES in Fig. 8 is in quite good agreement with experiments for z=10 mm, confirming that the discrepancies for $\bar{\mathcal{S}}^l$ are due to an overestimation of soot presence. On the contrary, at a higher axial position (z=30 mm) the LES predicts almost no soot. This situation represents a possible but not probable state visualized by the experiments. Therefore, results from the present LES at z=30 mm can be considered as representative of a possible but unlikely experimental state. The overall LES agreement presented in this section may be considered as not satisfactory. However, the final scope is not the validation of the shown LES results but to prove the potential of a new validation strategy accounting for the variability of time-averaged quantities when considering small time-averaging periods.

6. Conclusion

Achieving temporal convergence represents a challenge for LES of realistic turbulent configurations featuring low frequency flow motions and intermittent soot production. In this work, high-speed measurements were employed to demonstrate that a statistically converged solution cannot be obtained when considering too small time-averaging intervals similar to what is considered in LES. To overcome this issue, a paradigm change for the validation of LES results is proposed by considering high-speed LS measurements together with numerically synthesised signals. In particular, to validate an LES simulation it should be verified that the time-averaged numerical results can be considered as a realisation of possible time-averaged states observed in experiments for the equivalent averaging interval. For this, two elements were developed. First, the numerical synthesis of LS signals from instantaneous LES fields was proposed based on the same temporal and spatial resolutions in both experiments and simulations. A sampling procedure was developed to create a statistical representation of the time-averaged possible experimental states from high-speed measurements that can be used as a confidence chart for LES validation. By looking at their PDF, it is possible to quantify the fluctuations of time-averaged experimental quantities when considering small time-averaging periods. This demonstrates the limitations of the classical validation procedure for numerical simulations based on comparison of quantities time-averaged over different time ranges. The feasibility of the proposed validation strategy has been demonstrated by comparing

time-averaged LES results to the experimental confidence interval. It can be concluded that the considered LES results are one representation of a possible but unlikely experimental state of soot distribution in the DLR burner. It is worth mentioning that it is likely that many models will capture a possible state of a highly intermittent phenomenon. Therefore, very different models would be finally considered as valid using such statistical strategy. However, this work points out that in soot intermittent configurations the validation and comparison of numerical models based on time-averaged results are neither rigorous nor fair, and thus could validate or discard models for the wrong reasons. On the contrary, to increase the fidelity of the conclusions, the simulation would have to be performed for an extended runtime and the resultant time-averaged profile should be compared again to the corresponding PDFs. Additional statistical post-processing procedures, such as the analysis of timescales using Fourier transform or considering time-averaging period of different lengths, can also be considered in future. Finally, the proposed approach exemplifies the unexplored potential of high-speed measurements to validate LES results for any rare combustion event characterized by long time scales, such as soot production but also local extinction or thermo-acoustic instabilities.

Acknowledgments

The authors gratefully acknowledge funding from the European Union within the SOPRANO H2020 project under Grant Agreement No. 690724. This work was performed using HPC resources from GENCI-CINES (Grant 2021-A0112B12029). B. Franzelli acknowledges the support of the European Research Council (ERC) under the European Union's Horizon 2020 research and innovation programme (Grant Agreement No. 757912).

Supplementary material

Supplementary material has been submitted.

References

[1] C. Dasch, D. Heffelfinger, Planar imaging of soot formation in turbulent ethylene diffusion flames: fluctuations and integral scales, Combust. Flame 85 (1991) 389–402.

[2] Y. Xin, J. P. Gore, Two-dimensional soot distributions in buoyant turbulent fires, Proc. Combust. Inst. 30 (2005) 719 – 726.

[3] D. O. Lignell, J. H. Chen, P. J. Smith, T. Lu, C. K. Law, The effect of flame structure on soot formation and transport in turbulent nonpremixed flames using direct numerical simulation, Combust. Flame 151 (2007) 2–28.

[4] S.-Y. Lee, S. R. Turns, R. J. Santoro, Measurements of soot, OH, and PAH concentrations in turbulent ethylene/air jet flames, Combust. Flame 156 (2009) 2264 – 2275.

[5] N. H. Qamar, Z. T. Alwahabi, Q. N. Chan, G. J. Nathan, D. Roekaerts, K. D. King, Soot volume fraction in a piloted turbulent jet non-premixed flame of natural gas, Combust. Flame 156 (2009) 1339 – 1347.

[6] A. Attili, F. Bisetti, M. E. Mueller, H. Pitsch, Formation, growth, and transport of soot in a three-dimensional turbulent non-premixed jet flame, Combust. Flame 161 (2014) 1849 – 1865.

[7] P. G. Arias, V. R. Lecoustre, S. Roy, Z. Luo, D. C. Haworth, T. Lu, A. Trouvé, H. G. Im, Dynamics of flow–soot interaction in wrinkled non-premixed ethylene–air flames, Combust. Theor. Model. 19 (2015) 568–586.

[8] B. Franzelli, P. Scouflaire, S. Candel, Time-resolved spatial patterns and interactions of soot, PAH and OH in a turbulent diffusion flame, Proc. Combust. Inst. 35 (2015) 1921 – 1929.

[9] K. P. Geigle, R. Hadef, M. Stöhr, W. Meier, Flow field characterization of pressurized sooting swirl flames and relation to soot distributions, Proc. Combust. Inst. 36 (2017) 3917 – 3924.

[10] M. Stöhr, K. Geigle, R. Hadef, I. Boxx, C. Carter, M. Grader, P. Gerlinger, Time-resolved study of transient soot formation in an aero-engine model combustor at elevated pressure, Proc. Combust. Inst. 37 (2019) 5421–5428.

[11] M. Grader, Z. Yin, K. P. Geigle, P. Gerlinger, Influence of flow field dynamics on soot evolution in an aero-engine model combustor, Proc. Combust. Inst. 38 (2021) 6421–6429.

[12] L. Tardelli, N. Darabiha, D. Veynante, B. Franzelli, Validating soot models in LES of turbulent flames: The contribution of soot subgrid intermittency model to the prediction of soot production in an aero-engine model combustor, Proc. ASME TurboExpo 2021, GT2021-60296, ASME, 2021.

[13] A. Felden, E. Riber, B. Cuenot, Impact of direct integration of analytically reduced chemistry in LES of a sooting swirled non-premixed combustor, Combust. Flame 191 (2018) 270 – 286.

[14] C. Eberle, P. Gerlinger, K. P. Geigle, M. Aigner, Toward finite-rate chemistry large-eddy simulations of sooting swirl flames, Combust. Sci. Technol. 190 (2018) 1194–1217.

[15] M. Grader, C. Eberle, P. Gerlinger, M. Aigner, LES of a pressurized, sooting aero-engine model combustor at different equivalence ratios with a sectional approach for PAHs and soot, Proc. ASME TurboExpo 2018, GT2018-75254, ASME, 2018.

[16] S. T. Chong, M. Hassanaly, H. Koo, M. E. Mueller, V. Raman, K. P. Geigle, Large eddy simulation of pressure and dilution-jet effects on soot formation in a model aircraft swirl combustor, Combust. Flame 192 (2018) 452 – 472.

[17] B. Franzelli, A. Vié, N. Darabiha, A three-equation model for the prediction of soot emissions in LES of gas turbines, Proc. Combust. Inst. 37 (2019) 1344 – 1363.

[18] L. Gallen, A. Felden, E. Riber, B. Cuenot, Lagrangian tracking of soot particles in LES of gas turbines, Proc. Combust. Inst. 37 (2019) 5429 – 5436.

[19] K. P. Geigle, M. Köhler, W. O'Loughlin, W. Meier, Investigation of soot formation in pressurized swirl flames by laser measurements of temperature, flame structures and soot concentrations, Proc. Combust. Inst. 35 (2015) 3373 – 3380.

[20] J. Pinson, D. Mitchell, R. Santoro, T. Litzinger, Mod-

eling atomization and break up in high-pressure diesel sprays, SAE Paper 932650 (1993).
[21] M. Köhler, I. Boxx, K. P. Geigle, W. Meier, Simultaneous planar measurements of soot structure and velocity fields in a turbulent lifted jet flame at 3 kHz, Appl. Phys. B 103 (2011) 271–279.
[22] J. B. Michael, P. Venkateswaran, C. R. Shaddix, T. R. Meyer, Effects of repetitive pulsing on multi-khz planar laser-induced incandescence imaging in laminar and turbulent flames, Appl. Opt. 54 (2015) 3331–3344.
[23] K. P. Geigle, R. Hadef, W. Meier, Soot formation and flame characterization of an aero-engine model combustor burning ethylene at elevated pressure, J. Eng. Gas Turb. Power 136 (2013) 021505.
[24] T. Schönfeld, M. Rudgyard, A cell-vertex approach to local mesh refinement for the 3-d euler equations, 32nd Aerospace Sciences Meeting & Exhibit, AIAA-94-0318, AIAA, 1994.
[25] M. Ihme, H. Pitsch, Modeling of radiation and nitric oxide formation in turbulent nonpremixed flames using a flamelet/progress variable formulation, Phys. Fluids 20 (2008) 055110.
[26] P. Nau, Z. Yin, K.P. Geigle, W. Meier, Wall temperature measurements at elevated pressures and high temperatures in sooting flames in a gas turbine model combustor, Appl. Phys. B 123 (2017) 279.
[27] B. Connelly, M. Long, M. Smooke, R. Hall, M. Colket, Computational and experimental investigation of the interaction of soot and NO in coflow diffusion flames, Proc. Combust. Inst. 32 (2009) 777 – 784.
[28] A. Bodor, A. Cuoci, T. Faravelli, B. Franzelli, A forward approach for the validation of soot sizing models using laser-induced incandescence, Appl. Phys. B 126 (2020) 49.